Electronic Supplementary Information:

Nature of Ultrafast Dynamics in the Lowest-Lying Singlet Excited State of $[Ru(bpy)_3]^{2+}$

Chenyu Zeng, Yaqi Li, Hangjing Zheng, Mingxing Ren, Wei Wu and Zhenhua Chen*

State Key Laboratory of Physical Chemistry of Solid Surfaces, Fujian Provincial Key Laboratory of Theoretical and Computational Chemistry, College of Chemistry and Chemical Engineering, Xiamen University, Xiamen, Fujian 361005, China

*Email: zhhchen@xmu.edu.cn

Contents

S1 Computational Details

A. Vibrational Relaxation Time

In the vibrational relaxation of the $^1MLCT_1$ state from the Franck-Condon point to its equilibrium geometry, the bpy ligand, on which the excited electron is located, displays the main geometric distortion, and the bridged C-C bond length shows the largest change. This bond length change was taken as the vibrational displacement as a simple approximation, namely that the distance of intramolecular vibrational relaxation is about 0.051 Å. Further, the average velocity of the vibrational relaxation can be inferred from the characteristic normal mode associated with the process. This normal mode is listed in Table S4. It is obtained by matching the abovementioned geometric distortion with each normal mode at the $^1MLCT_1$ state equilibrium geometry. The amplitude of the characteristic normal mode is also represented by the change of bridged C-C bond length, estimated to be ca. 0.425 Å. The vibrational velocity at the equilibrium geometry, 2.114×10^{13} Å/s, is calculated by using the vibrational frequency, 4.98×10^{13} s^{-1}. The average velocity of vibrational relaxation is approximately taken as half of the velocity at equilibrium geometry, namely 1.057×10^{13} Å/s, considering that at the Franck-Condon point, the characteristic normal mode has an imaginary frequency and thus the vibrational velocity is slower. Then, by using the vibrational distance and the average velocity, the vibrational relaxation time is estimated to be only about 5 fs.

B. Probabilities of Adiabatic and Nonadiabatic Electron Transfers

From the Landau-Zener model, the adiabatic transition probability P can be written as

$$P = 1 - \exp\left[-\frac{4\pi^2 V_{12}^2}{hv\left|\mathbf{s}_1 - \mathbf{s}_2\right|} \right], \quad (1)$$

where h is the Planck constant, v is the nuclear velocity during the reaction, V_{12} is the electronic coupling between the two diabatic states and $|\mathbf{s}_1\text{-}\mathbf{s}_2|$ is the difference of the slopes of the two diabatic PESs at the crossing point.

The electronic coupling V_{12} is approximated equal to one-half of the energy gap between the $^1MLCT_1$ and $^1MLCT_2$ states at the transition state geometry, based on the two-state model.

The nuclear velocity v is estimated by the thermally averaged approximation,

$$v = \sqrt{2k_B T / \pi\mu}, \quad (2)$$

where k_B is the Boltzmann constant (1.380649×10^{-23} J/K), T the temperature is at 298.15 K, and μ is the reduced mass.

The slope difference $|\mathbf{s}_1\text{-}\mathbf{s}_2|$ is calculated by using the harmonic oscillator approximation,

$$\left|\mathbf{s}_1 - \mathbf{s}_2\right| = \sqrt{2\lambda f}, \quad (3)$$

where λ represents the reorganization energy, and f is the force constant of the relevant vibrational mode at the equilibrium geometry.

Among the above parameters, the reduced mass μ and the force constant f are obtained from TDDFT frequency computation, which are 1.747×10^{-26} kg and 914.69 J/m^2, respectively. On the other hand, the electronic coupling V_{12} and the reorganization energy λ, 0.54 and 12.47 kcal/mol, respectively, are both obtained from averaged results of TDDFT and CASSCF methods. As a comparison, the results of several other methods are listed in Table S1. Using these parameters, the nuclear velocity v is 387.27 m/s as was calculated from Eq. (2), and the difference of slopes $|\mathbf{s}_1\text{-}\mathbf{s}_2|$ is ca. 1.26×10^{-8} J/m from Eq. (3). Finally, the probability P of adiabatic ILET is about 16% from Eq. (1). Therefore, the probability of nonadiabatic transfer is 84%.

Table S1. The electronic coupling and the reorganization energy calculated by several methods. All values are given in kcal/mol.

	TDDFT	CASSCF	CASPT2	RASCI	RASPT2	This work [a]
V_{12}	0.88	0.21	2.94	0.17	1.54	0.54
λ	9.75	15.20	18.20	14.05	17.17	12.47

a. This work employs the average results obtained from TDDFT and CASSCF methods. The two-state model might not be applicable to CASPT2 and RASPT2 methods, since the reference-state weights in both methods are quite small, only 0.34. Therefore, these two methods are not used for the electronic coupling and the reorganization energy, even though they are more accurate in energy evaluation. Meanwhile, all the remaining three methods, TDDFT, CASSCF and RASCI, have only one dominant configuration state function whose coefficient is exceeding 0.97, indicating that the two-state model is applicable to these methods. However, both CASSCF and RASCI methods address very limited dynamic electronic correlation energy and might underestimate the energy gap between adiabatic states. Hence, the electronic coupling is calculated by averaging the results of TDDFT and CASSCF methods. For consistency, the reorganization energy is also obtained by a similar average.

C. Electron Transfer Rate

The electron transfer rate constant, k_{et}, is calculated by the classical transition state formalism,

$$k_{et} = \upsilon_{eff}\kappa_{el}\exp(-\Delta G^*/k_B T), \quad (4)$$

where υ_{eff} is the effective vibrational frequency, κ_{el} is the electronic factor, ΔG^* is the activation free energy, and k_B and T are the Boltzmann constant and the temperature, respectively.

The effective vibrational frequency υ_{eff} is calculated by using the harmonic oscillator approximation, which is the frequency of the relevant normal mode (Figure S6) at the equilibrium geometry.

The electronic factor κ_{el} for a nonadiabatic electron transfer reaction can be expressed as

$$\kappa_{el} = 2P/(1+P), \quad (5)$$

where P represents the probability of adiabatic electron transfer given in Eq. (1).

The activation free energy ΔG^* is defined as the difference between the free energy G of the $^1MLCT_1$ state at the transition state and the equilibrium geometries. In general, G can be expressed as

$$G = E + ZPE + \Delta G_{0\rightarrow T}, \quad (6)$$

where E is the electronic energy, ZPE is the zero-point energy and $\Delta G_{0\rightarrow T}$ takes into account the effect of temperature on free energy. The sum of the last two terms gives the thermal correction of free energy.

Among the above parameters, the electronic factor κ_{el} 0.276 is calculated by substituting the probability P (16%) into Eq. (5). The effective vibrational frequency and the thermal correction are both obtained from TDDFT frequency calculation. The former, $\upsilon_{eff} = 4.98\times10^{13}$ s^{-1}, is estimated at the equilibrium geometry, while the latter are 267.22 and 269.43 kcal/mol, respectively, at the transition state and the equilibrium geometries. The electronic energy E is calculated with several methods. For comparison, Table S2 lists the electronic energy barrier and the activation free energy calculated by several methods. From the results, it can be seen that the electron transfer may have a very limited barrier or even be barrierless. Therefore, in this work, the exponential term

exp(-$\Delta G^*/k_B T$) is approximately taken as 1, meaning that all reactants are active and can pass through the barrier. Then by using these parameters, the electron transfer rate constant, $k_{et} = 1.38\times10^{13}$ s^{-1}, is derived from Eq. (4).

Table S2. The electronic energy barrier and the activation free energy calculated by several methods. All values are given in kcal/mol.

	TDDFT	CASSCF	CASPT2	RASCI	RASPT2	This work [a]
ΔE	2.09	5.23	-1.39	4.91	0.94	/
ΔG^*	-0.12	3.03	-3.59	2.71	-1.26	0

a. This work takes ILET as a barrierless process. The CASSCF and RASCI methods, which do not address sufficient dynamic electron correlation, are often less accurate in estimating energy barriers. Therefore, their results are excluded. For general applications, TDDFT, CASPT2, and RASPT2 methods are considered to be able to adequately address dynamic electron correlation. However, these methods predict negative ΔG^* values, and the CASPT2 method even produces negative ΔE. These are in contradiction to the chemical intuition that ΔG^* shall be nonnegative. From the present results, it is quite safe to propose that ILET has an extremely small barrier if it is not barrierless, and hence vanishing ΔG^* is used in this work for simplicity.

Table S3. The main geometric parameters for several characteristic geometries.[a]

Points [b]	bpy_a			bpy_b			bpy_c		
	$Ru\text{-}N_1$	$Ru\text{-}N_2$	$C\text{-}C_a$	$Ru\text{-}N_3$	$Ru\text{-}N_4$	$C\text{-}C_b$	$Ru\text{-}N_5$	$Ru\text{-}N_6$	$C\text{-}C_c$
O	2.055	2.055	1.469	2.055	2.055	1.469	2.055	2.055	1.469
a	2.042	2.042	1.418	2.049	2.068	1.468	2.068	2.049	1.468
TS_{ab}	2.045	2.038	1.441	2.038	2.045	1.441	2.065	2.065	1.468
O′	2.047	2.047	1.449	2.047	2.047	1.449	2.047	2.047	1.449

a. $C\text{-}C_a$ to $C\text{-}C_c$ represent the bridged C-C bond in the bpy_a to bpy_c, respectively. Bond lengths are given in Å.

b. From top to bottom, they are the ground state geometry, the $^1MLCT_1$ state minima **a**, the transition state geometry between **a** and **b**, and $^1MLCT_1$ state geometry constrained by D_3 symmetry.

Table S4. The normal mode for vibrational relaxation and ILET at the $^1MLCT_1$ state equilibrium geometry.

Ru	-0.00	0.00	-0.00	C	-0.06	-0.02	-0.06
N	0.01	0.00	-0.01	C	0.07	0.06	0.08
C	-0.01	-0.00	0.01	H	-0.17	0.23	-0.18
C	0.00	0.01	-0.01	H	0.12	0.24	0.14
C	-0.01	-0.00	0.01	H	0.05	0.15	0.06
C	0.01	0.00	-0.00	H	0.14	-0.05	0.16
C	-0.00	-0.00	0.01	H	0.17	0.23	0.18
N	-0.00	0.01	-0.01	H	-0.12	0.24	-0.14
C	0.01	-0.01	0.00	H	-0.05	0.15	-0.06
C	-0.00	0.01	-0.01	H	-0.14	-0.05	-0.16
C	0.01	-0.02	0.01	N	-0.01	0.00	0.01
C	-0.01	0.01	-0.01	C	0.01	-0.00	-0.01
C	0.00	-0.01	0.01	C	-0.00	0.01	0.01
H	0.01	-0.01	0.01	C	0.01	-0.00	-0.01
H	0.02	0.00	-0.01	C	-0.01	0.00	0.00
H	0.00	0.00	-0.01	C	0.00	-0.00	-0.01
H	-0.00	0.01	-0.00	N	0.00	0.01	0.01
H	-0.01	0.01	-0.00	C	-0.01	-0.01	-0.00
H	-0.01	0.02	-0.02	C	0.00	0.01	0.01
H	0.02	0.00	-0.01	C	-0.01	-0.02	-0.01
H	0.02	0.00	-0.01	C	0.01	0.01	0.01
N	0.05	0.01	0.06	C	-0.00	-0.01	-0.01
C	-0.14	0.00	-0.16	H	-0.01	-0.01	-0.01
C	0.18	-0.03	0.20	H	-0.02	0.00	0.01
C	-0.16	-0.07	-0.18	H	-0.00	0.00	0.01
C	0.06	-0.02	0.06	H	0.00	0.01	0.00
C	-0.07	0.06	-0.08	H	0.01	0.01	0.00
N	-0.05	0.01	-0.06	H	0.01	0.02	0.02
C	0.14	0.00	0.16	H	-0.02	0.00	0.01
C	-0.18	-0.03	-0.20	H	-0.02	0.00	0.01
C	0.16	-0.07	0.18				

Table S5. The normal mode for ILET at the transition state geometry.

Ru	-0.00	0.00	-0.00	C	-0.10	-0.11	-0.02
N	-0.02	0.01	0.00	C	-0.02	0.07	-0.05
C	-0.00	0.00	-0.00	H	0.00	-0.00	0.00
C	-0.00	-0.01	-0.00	H	-0.02	0.03	-0.01
C	-0.00	0.00	0.00	H	-0.04	-0.02	0.03
C	0.01	-0.00	-0.00	H	0.08	0.04	0.19
C	-0.02	0.00	-0.00	H	-0.00	0.00	-0.00
N	0.02	0.01	0.00	H	0.02	0.01	0.03
C	0.00	0.00	-0.00	H	-0.03	-0.06	0.00
C	0.00	-0.01	-0.00	H	-0.06	0.06	-0.06
C	0.00	0.00	0.00	N	0.08	-0.11	-0.04
C	-0.01	-0.00	-0.00	C	-0.20	-0.07	0.26
C	0.02	0.00	-0.00	C	0.04	0.10	-0.11
H	0.00	0.01	-0.01	C	-0.12	0.03	0.09
H	0.00	0.01	-0.01	C	0.10	-0.11	-0.02
H	-0.01	0.00	-0.02	C	0.02	0.07	-0.05
H	-0.05	0.00	-0.09	C	0.14	0.17	-0.25
H	-0.00	0.01	-0.01	N	0.07	-0.09	0.06
H	-0.00	0.01	-0.01	C	-0.11	-0.00	0.11
H	0.01	0.00	-0.02	C	0.01	0.13	-0.10
H	0.05	0.00	-0.09	C	0.06	-0.14	0.03
N	-0.07	-0.09	0.06	C	-0.08	0.02	0.06
C	-0.14	0.17	-0.25	H	0.00	0.00	-0.00
C	0.11	-0.00	0.11	H	-0.02	0.01	0.03
C	-0.01	0.13	-0.10	H	0.03	-0.06	0.00
C	-0.06	-0.14	0.03	H	0.06	0.06	-0.06
C	0.08	0.02	0.06	H	-0.00	-0.00	0.00
N	-0.08	-0.11	-0.04	H	0.02	0.03	-0.01
C	0.20	-0.07	0.26	H	0.04	-0.02	0.03
C	-0.04	0.10	-0.11	H	-0.08	0.04	0.19
C	0.12	0.03	0.09				

Table S6. The relative energies (kcal/mol) and oscillator strengths (in parentheses) of $^1MLCT_{1\text{-}3}$ states obtained at the ground state equilibrium geometry.

	TDDFT	RASCI	SA-CASSCF[a]	RASPT2	CASPT2
$^1MLCT_1$	0.00 (1.0×10^{-4})	0.00 (4.6×10^{-3})	0.00 (5.1×10^{-4})	0.00	0.00
$^1MLCT_2$	0.00 (1.0×10^{-4})	0.00 (4.6×10^{-3})	0.00 (5.1×10^{-4})	0.34	1.10
$^1MLCT_3$	0.29 (1.1×10^{-3})	2.17 (1.7×10^{-2})	3.62 (4.1×10^{-3})	3.33	8.50

a. SA-CASSCF uses the same active space as RASCI with orbitals further optimized. In addition to the ground state and nine ^{1}MLCT states, three π→π* and six d→d* states are further included, resulting in nineteen states in total. Two different weights are used for these states, i.e. the π→π* state has twice weight of other states.

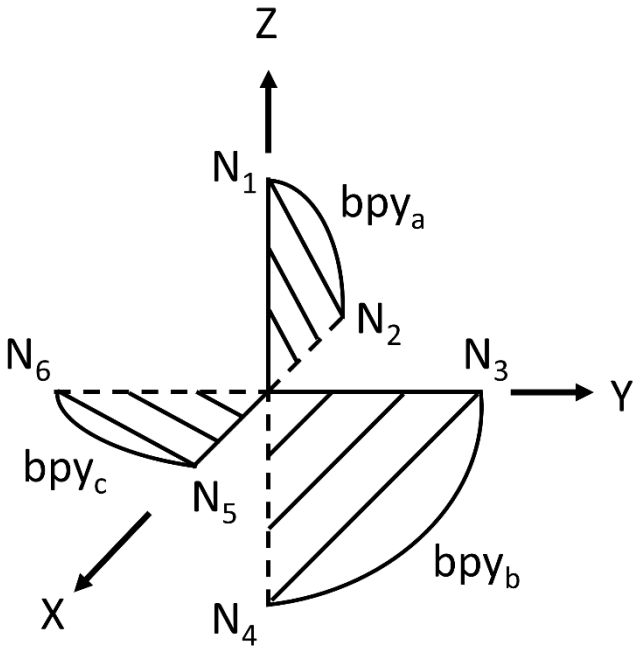

Figure S1. Molecular orientation of the $[Ru(bpy)_3]^{2+}$ complex. The Ru atom is placed at the center, and the three bpy ligands are arranged as much as possible on a plane formed by coordinate axes. Each bpy ligand is further abstractly represented by a shadowed sector. The solid lines represent positive axes, and the dashed lines denote negative axes.

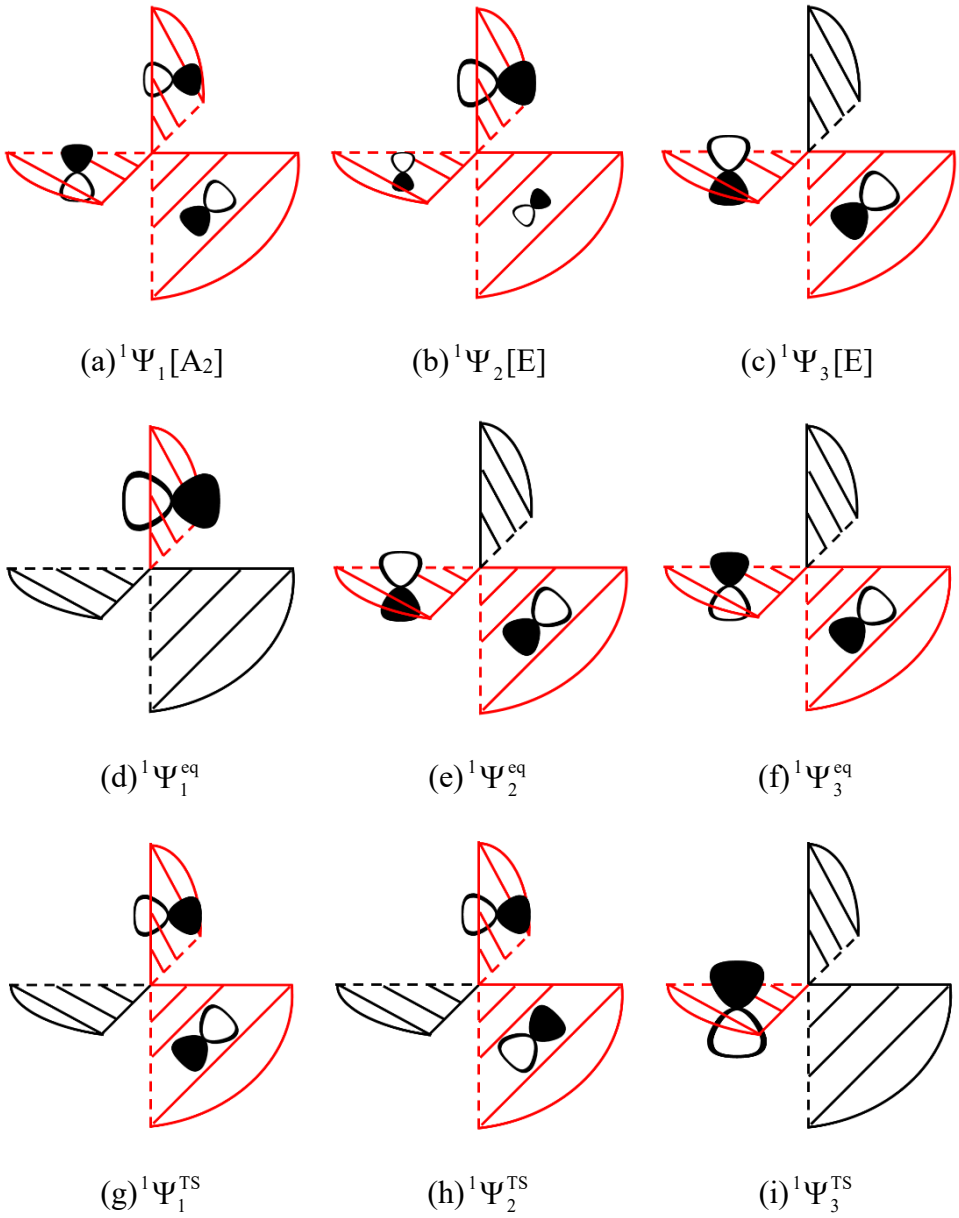

Figure S2. Schematic diagrams of adiabatic wave functions of ^{1}MLCT$_{1\text{-}3}$ states at the ground state equilibrium (a-c), ^{1}MLCT$_1$ state equilibrium (d-f) and transition state (g-i) geometries. These adiabatic states are primarily composed of a symmetry-adapted linear combination of diabatic states Φ_a^d, Φ_b^d and Φ_c^d, namely that (a) $^1\Psi_1 = \Phi_a^d + \Phi_b^d + \Phi_c^d$, (b) $^1\Psi_2 = 2\Phi_a^d - \Phi_b^d - \Phi_c^d$, (c) $^1\Psi_3 = \Phi_b^d - \Phi_c^d$, (d) $^1\Psi_1^{eq} = \Phi_a^d$, (e) $^1\Psi_2^{eq} = \Phi_b^d - \Phi_c^d$, (f) $^1\Psi_3^{eq} = \Phi_b^d + \Phi_c^d$, (g) $^1\Psi_1^{TS} = \Phi_a^d + \Phi_b^d$, (h) $^1\Psi_2^{TS} = \Phi_a^d - \Phi_b^d$ and (i) $^1\Psi_3^{TS} = \Phi_c^d$. The symmetries of these states are given in square brackets. Here and after,

the sizes of p-type orbitals approximately reflect the relative magnitudes of the coefficients of the corresponding diabatic wave functions.

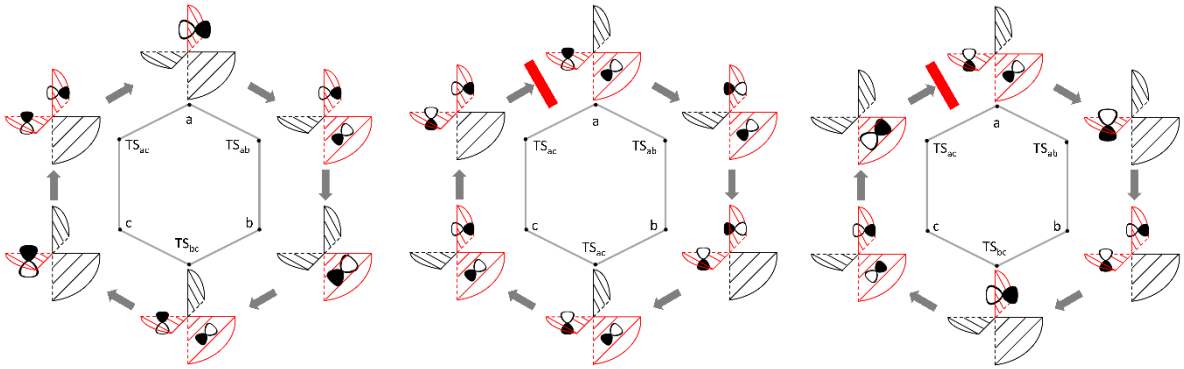

(1) (2) (3)

Figure S3. Diagrammatic representation of the evolutions of adiabatic wave functions along a loop of ILETs. Diagrams (1)-(3) are for $^1\Psi_1$-$^1\Psi_3$, respectively. The points **a**, **b** and **c** denote the three minima of the ^{1}MLCT$_1$ state. The points **TS$_{ab}$**, **TS$_{bc}$** and **TS$_{ac}$** represent the transition state geometries between **a** and **b**, **b** and **c**, and **a** and **c**, respectively. The wave function of ^{1}MLCT$_1$ state keeps invariant but the phases of both ^{1}MLCT$_2$ and ^{1}MLCT$_3$ states are reversed, denoted by a solid red line, when the molecular geometries gradually change along the loop **a**→**TS$_{ab}$**→**b**→**TS$_{bc}$**→**c**→**TS$_{ac}$**→**a**.

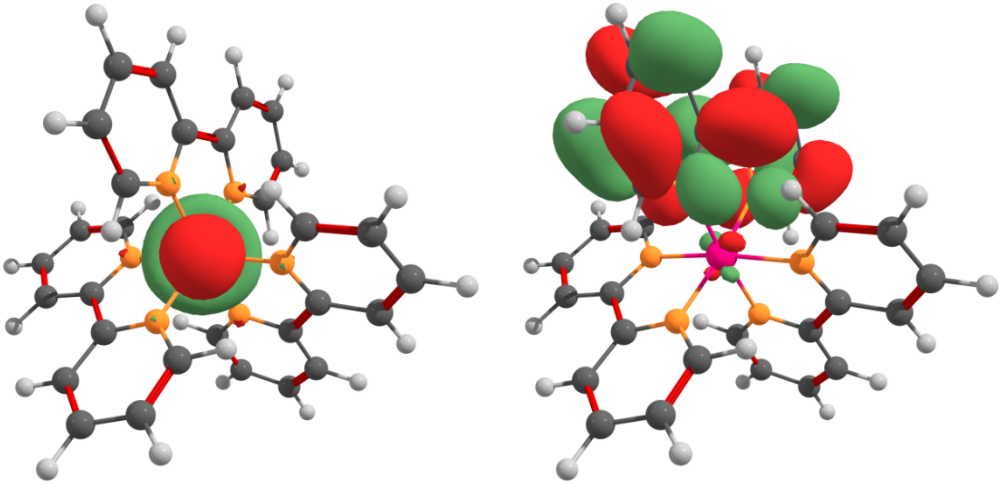

(a) d_1 (b) π_{la}*

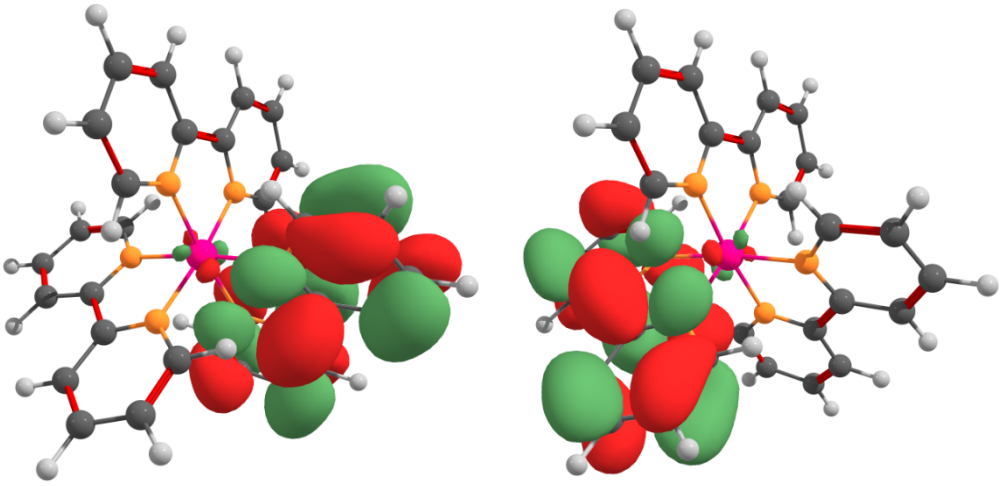

(c) π_{lb}* (d) π_{lc}*

Figure S4. Localized orbitals for diabatic states. The ligand π* orbitals (b)-(d) were obtained from a localization of ligand group orbitals. These orbitals are almost unchanged during the ILET process.

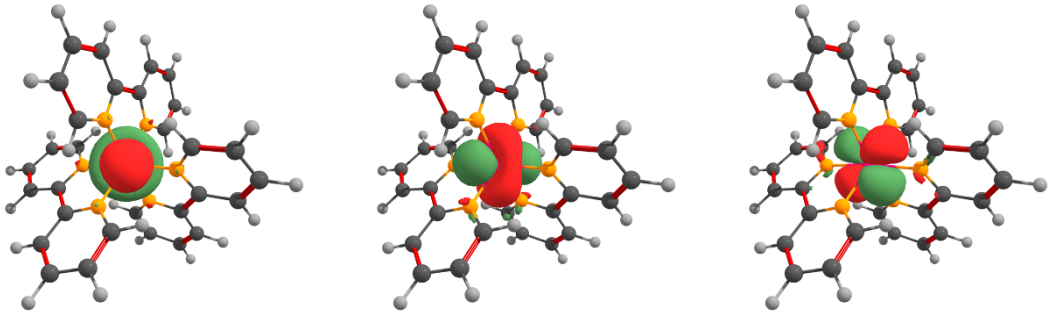

(a) d_1 (b) d_2 (c) d_3

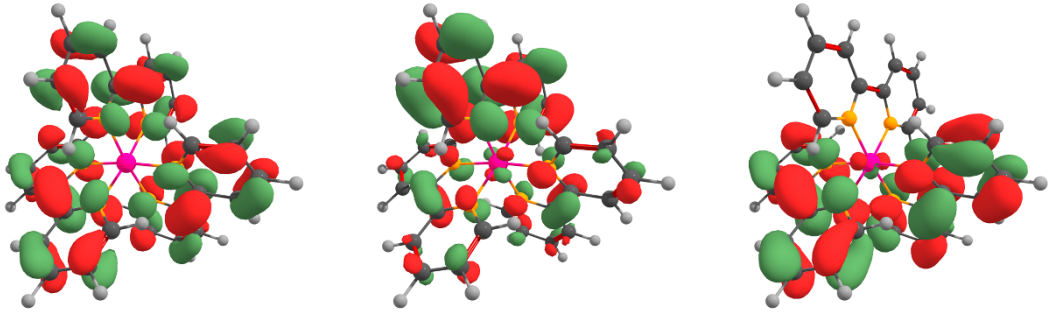

(d) π_1* (e) π_2* (f) π_3*

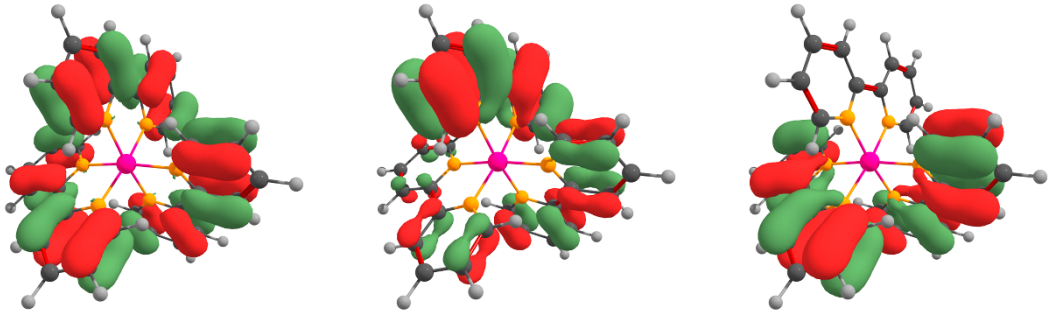

(g) π_1 (h) π_2 (i) π_3

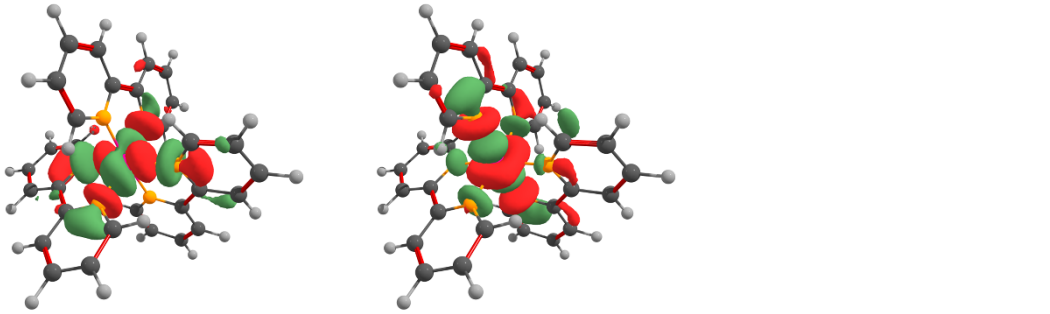

(j) d_1* (k) d_2*

Figure S5. The active orbitals for multiconfigurational and multireference calculations. These orbitals are optimized by CASSCF method. The subsequent CASPT2, RASCI(12,11) and RASPT2 computations also employ these orbitals. In RASCI, RAS2

orbital subspace consists all six active orbitals in CASSCF (6,6), shown as Ru-4d(t2g) orbitals (a-c) and the ligand group orbitals (d-f). RAS1 and RAS3 subspaces include three ligand π orbitals (g-i) and two metal dσ* orbitals (j-k), respectively.

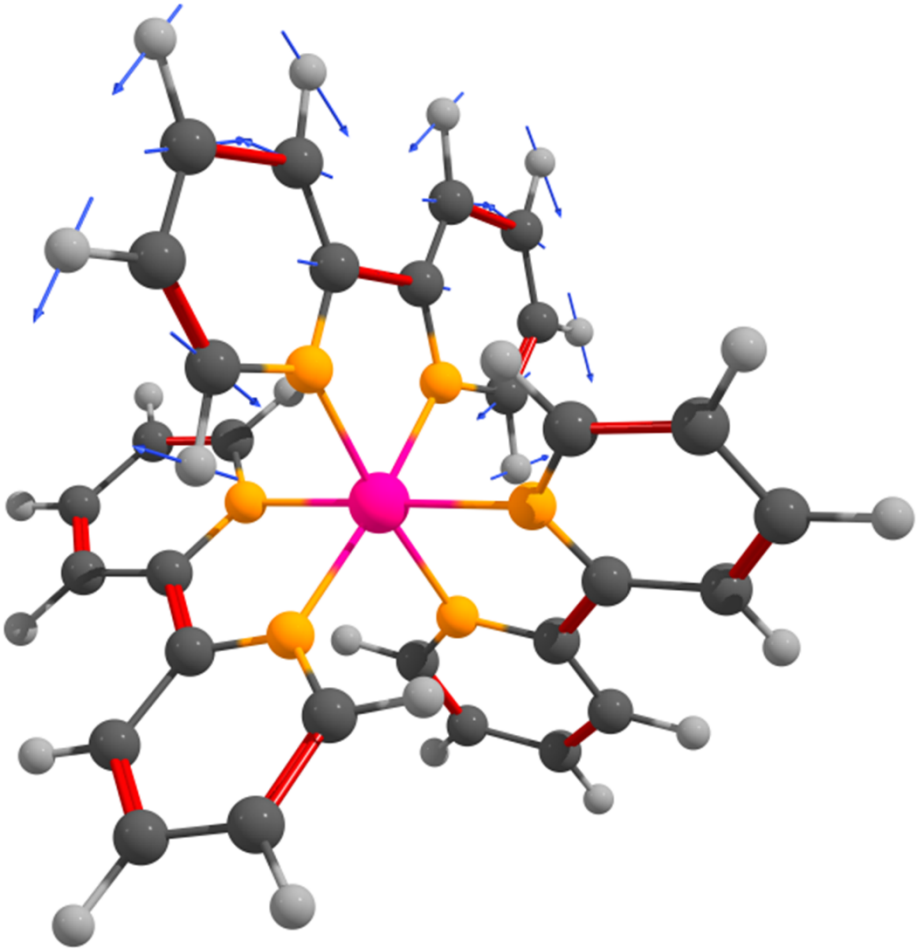

Figure S6. The vibration relaxation mode at the equilibrium geometry of $^{1}MLCT_{1}$ state.